Thin Solid Films 519 (2011) 5178–5182

Contents lists available at ScienceDirect

Thin Solid Films

journal homepage: www.elsevier.com/locate/tsf

Improved properties of Ti-doped ZnO thin films by hydrogen plasma treatment

F.H. Wang *, H.P. Chang, J.C. Chao

Department of Electrical Engineering and Graduate Institute of Optoelectronic Engineering, National Chung Hsing University, Taichung, Taiwan, ROC

ARTICLE INFO

Available online 15 January 2011

Keywords:
Ti-doped zinc oxide (TZO)
Sputter
Substrate temperature
Hydrogen plasma

ABSTRACT

This work investigates the effects of substrate temperature (T_S) and hydrogen plasma post-treatment on the properties of TZO thin films prepared by radio frequency magnetron sputter. All films had a (002) preferential orientation along the c axis at 2θ~34°. As T_S increased from room temperature to 300 °C, the structural, electrical, and optical characteristics of the TZO films were enhanced. The hydrogen plasma was performed by a plasma-enhanced chemical vapor deposition system at 300 °C. The film resistivity decreased markedly by 60% to 1.20×10^{-3} Ω cm after a 90-min treatment in comparison with that of the as-deposited film. The improved characteristics of the plasma-treated TZO films are attributed to the formation of shallow donors and the desorption of oxygen species at grain boundaries during hydrogen plasma treatment.

1. Introduction

Zinc oxide (ZnO) is an n-type semiconductor with a large binding energy of 60 meV and a wide bandgap of 3.3 eV in the UV range. ZnO has lots of applications in optoelectronic devices such as solar cells [1], light-emitting diodes [2], blue laser diodes [3], and flat-panel displays [4]. Doped ZnO films are promising alternatives to replace indium-tin-oxide (ITO) films as transparent conducting films due to their stable electrical and optical properties. The doping of Al [5,6], Ga [7,8], and In [9,10] in ZnO films has been widely studied to enhance n-type conductivity. The trivalent cation-doped ZnO films present good electrical conductivity and transparency over the visible spectrum. Few researches on quadrivalent cation-doped ZnO have been published. The quadrivalent cation can provide two free electrons to contribute the conductivity as it substitutes Zn in ZnO films. It has one more valence than the trivalent cation. Ti is a quadrivalent cation and has a radius of 68 pm which is close to that of Zn (74 pm). Thus, it is suitable as a donor in ZnO. Ti-doped ZnO (TZO) thin films have been prepared by several techniques, including radio frequency (RF)/DC sputtering [11–14], chemical vapor deposition (CVD) [15], and sol–gel process [16,17]. Among these methods, sputtering has advantages of good uniformity, high process controllability, and large-area deposition. The properties of TZO films are generally dependent on sputtering parameters such as substrate temperature, working pressure, type of substrate, and ambient gas. Lin et al. investigated the effect of the substrate temperature ranging from 50 to 200 °C on the properties of sputtered TZO films and indicated that the film resistivity decreased to a minimum of 9.69×10^{-3} Ω cm at 100 °C [14]. Chung et al. reported that the crystallinity of TZO films was improved with a low working pressure (5 mTorr) and a high substrate temperature (250 °C) and the lowest film resistivity (2.50×10^{-3} Ω cm) was obtained when the Ti addition was 1.34 wt.% [12]. Besides, Tsay et al. studied the properties of TZO films prepared by the sol–gel process and presented that the $Zn_{0.88}Ti_{0.12}O$ film exhibited high transmittance (91%) and small RMS roughness (1.04 nm) but relatively high resistivity (3.9×10^{6} Ω cm) [17]. In this study, RF magnetron sputtering with TiO_2-doped ZnO targets is used to investigate the effects of the substrate temperature on the structural, electrical, and optical properties of TZO films. In addition, a post-deposition hydrogen plasma treatment using the single-chamber plasma-enhanced CVD (PECVD) system is performed to further improve the electrical and optical properties of films because it is convenient and practical for large-area applications such as flat-panel displays and thin-film solar cells.

2. Experimental details

Zinc oxide powder mixed with 1.5 wt.% titanium oxide was sintered to be used as a sputter target. A 13.56 MHz RF magnetron sputtering source was installed in a deposition chamber to deposit a ceramic thin film. The TZO films with a thickness of about 330 nm were deposited on glass substrates (Corning 1737) at various substrate temperatures ranging from room temperature (RT) to 300 °C at an RF power of 100 W. The base pressure was 5×10^{-6} Torr and the working pressure was maintained at 5×10^{-3} Torr in Ar (99.995%) gas. After deposition, some of TZO films were treated by hydrogen plasma at an RF power of 80 W at a temperature of 300 °C for different exposure times.

The structure of TZO films was examined by X-ray diffraction (XRD) (PANalytical, 18 kW Rotating Anode X-ray Generator, Japan) analysis with Cu-Kα radiation (λ = 0.154056 nm). The morphology of TZO films was observed using field emission scanning electron microscopy (FE-SEM) (JEOL, JSM-6700) and atomic force microscopy

* Corresponding author. 250 Kuo-Kuang Rd., Taichung 40227, Taiwan. Tel.: +886 4 22851549x706; fax: +886 4 22851410.
E-mail address: fansen@dragon.nchu.edu.tw (F.H. Wang).

0040-6090/$ – see front matter © 2011 Elsevier B.V. All rights reserved.
doi:10.1016/j.tsf.2011.01.083

(AFM) (Digital Instrument, NS4/D3100CL/Multimode). The resistivity, Hall mobility, and carrier concentration were measured using the Van der Pauw method (BIO-RAD, HL5500IU) at RT. The optical transmittance was detected using a UV/VIS/IR spectrophotometer (Jasco V-570) in the 220–2500 nm wavelength range.

3. Results and discussion

Fig. 1 shows the deposition rate of the TZO films at various substrate temperatures. The film thickness was determined by spectroscopic ellipsometer (Nano View, SE MF-1000). The deposition rate is an important parameter for practical thin-film deposition. Results showed that the deposition rate increased slightly first and then decreased with increasing substrate temperature. The maximum deposition rate was 10.31 nm/min at 200 °C. The reduction in the deposition rate at a high temperature was attributed to the diffusive ability of atoms or molecules that increased with the increase of the substrate temperature [18]. This trend is similar with the earlier report [19].

Fig. 2(a) exhibits the XRD spectra of the TZO films deposited at substrate temperatures of RT, 100, 200, and 300 °C. All patterns exhibited a (002) preferential orientation along the c axis at diffraction angles (2θ) near 34° ± 0.3° and no characteristic peak of TiO_2 was found. The peak intensity increased with increasing substrate temperature, revealing that the film crystallinity was enhanced at a high temperature. The 2θ diffraction angle shifted from 33.8° to 34.3° as the substrate temperature increased from RT to 300 °C. It may be attributed to that more Ti atoms replace substitutional Zn at a high deposition temperature. Since the ionic radius of Ti^{4+} (68 pm) is smaller than that of Zn^{2+} (74 pm), the position of the (002) peak is expected to shift to a larger 2θ value.

Fig. 2(b) shows the full-width at half-maximum (FWHM) and crystal size of the TZO films for various substrate temperatures. The crystal size was estimated with Scherrer's formula [20],

$$D = \frac{0.94\lambda}{\beta\cos\theta}, \quad (1)$$

where λ = 0.154056 nm, D is crystal size and β is FWHM. The FWHM decreased with the increase of the substrate temperature, indicating the increase of the crystal size. The crystal size increased from 20.4 to 30.3 nm when the substrate temperature increased from RT to 300 °C. This phenomenon is similar to the previous report [14].

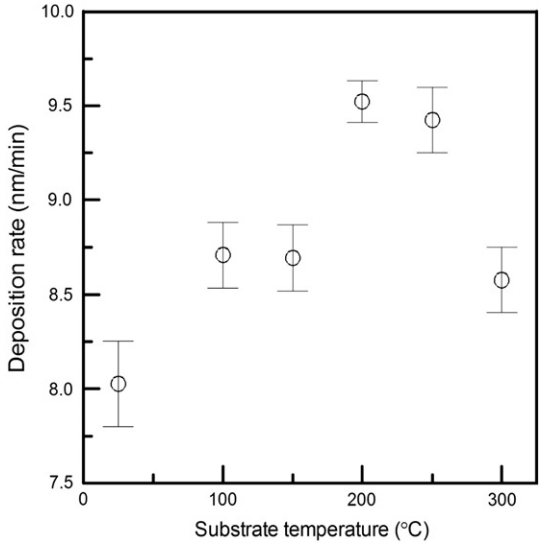

Fig. 1. Deposition rate of the TZO films as a function of substrate temperature.

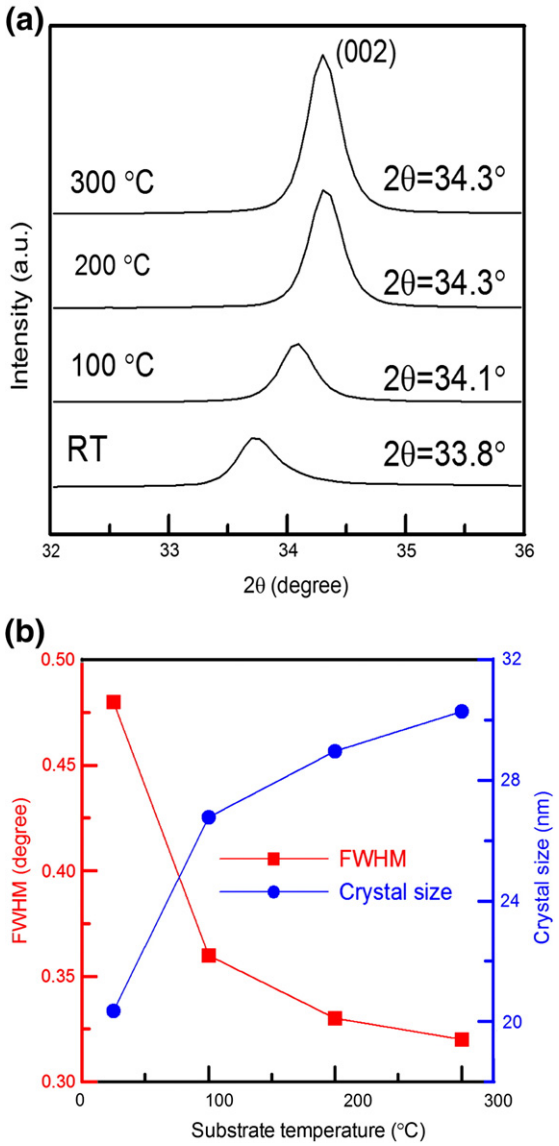

Fig. 2. (a) X-ray diffraction spectra and (b) FWHM and crystal size of the TZO films prepared at substrate temperatures of RT, 100, 200 and 300 °C.

Fig. 3 shows the FE-SEM images of the TZO films deposited at RT and 300 °C with a tilt angle of 45°. It was found that the surface morphology clearly altered with the substrate temperature. At a higher substrate temperature (300 °C), the film surface was smoother and the columnar structure appeared denser. The results of the XRD and SEM analysis suggest that the high substrate temperature increases the energy of adsorbed ions and thus improves the structural properties of TZO films.

Fig. 4 shows the resistivity, Hall mobility, and carrier concentration of the TZO films deposited at various substrate temperatures. The film resistivity decreased from 1.08 to 2.95×10^{-3} Ω cm when the substrate temperature increased from RT to 300 °C. Meanwhile, the carrier concentration and Hall mobility both increased from 8.64×10^{18} to 2.47×10^{20} cm^{-3} and 0.68 to 7.84 cm^2/Vs, respectively. At a substrate temperature of 300 °C, the resistivity, carrier concentration, and mobility attained the optimal values. The higher mobility and carrier concentration are due to better crystallinity and more intrinsic donors at a higher substrate temperature. The lower resistivity is achieved at a higher substrate temperature, as it occurs in the AZO films reported by Fang et al. [21]. However, Lin et al. [14] indicated that for the TZO film deposited at temperatures of 50–200 °C, the lowest resistivity was attained at 100 °C. They ascribed the

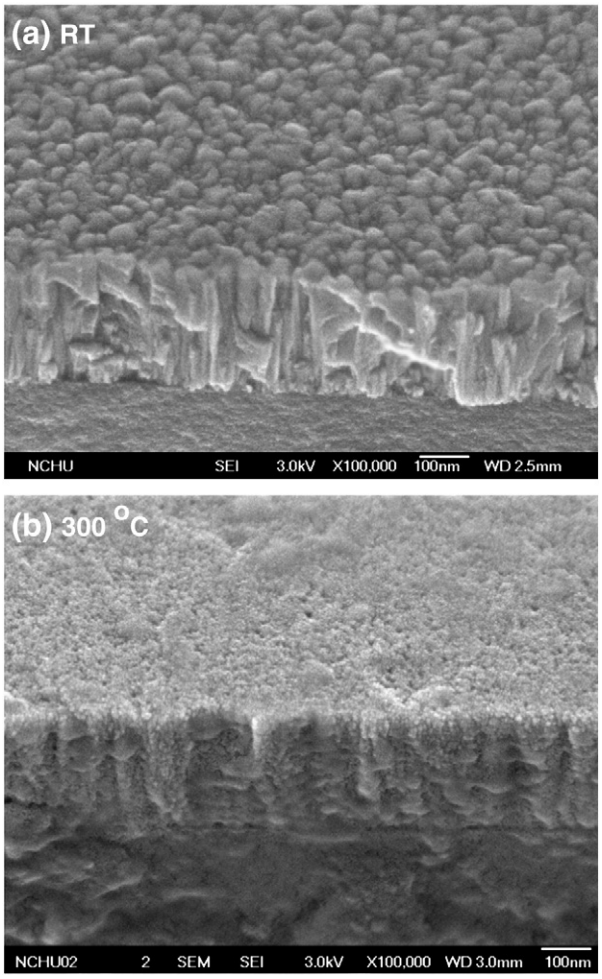

Fig. 3. FE-SEM images of the TZO films deposited at substrate temperatures of (a) RT and (b) 300 °C.

phenomenon to that re-evaporation at a high temperature possibly reduced the vacancies inside the film, thus causing the decrease in carrier concentration and mobility.

Fig. 5(a) and (b) shows the optical transmittance spectra and optical energy gap (Eg) of the TZO films prepared at various substrate temperatures. In Fig. 5(a), all films had high transmittances (>82%) in the visible wavelength region (400–700 nm) and a strong absorption in the UV region. The transmittance increased slightly with

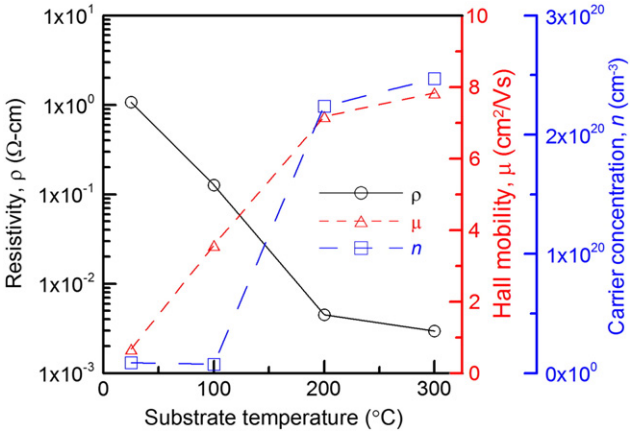

Fig. 4. Resistivity (ρ), Hall mobility (μ) and carrier concentration (n) of the TZO films as a function of the substrate temperature.

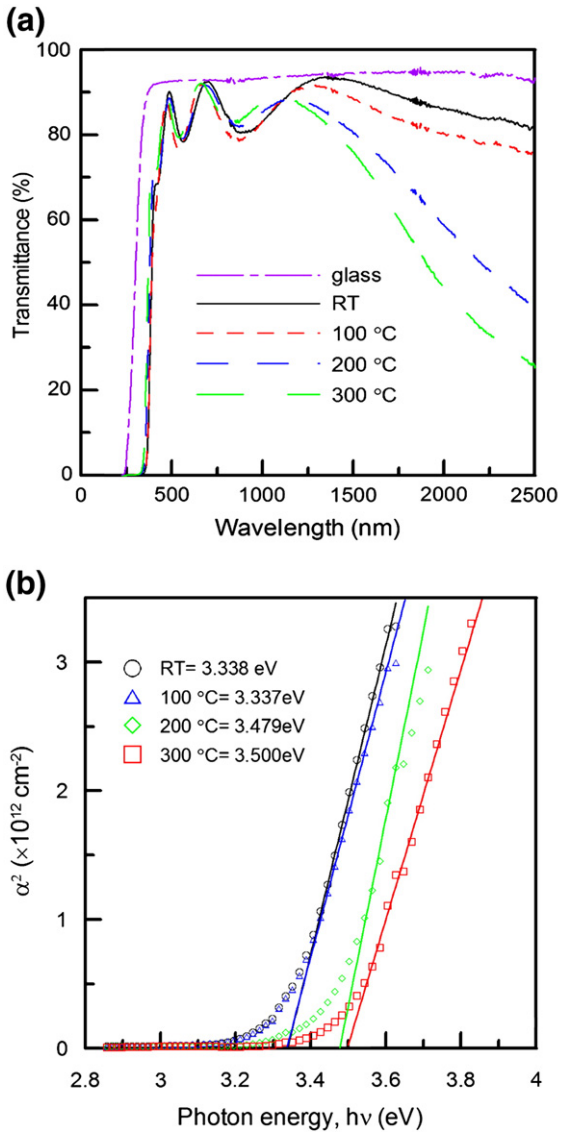

Fig. 5. (a) Optical transmittance spectra and (b) optical energy gap of TZO films prepared at various substrates temperatures.

the substrate temperature, and the average transmittances in the visible region for the films prepared at RT, 100, 200, and 300 °C were 82.8%, 82.2%, 83.1%, and 84.7%, respectively, while that of the glass substrate was 92.6%. Fig. 5(b) shows the α^2 vs. photon energy for the TZO films, where α is the optical absorption coefficient. The calculated Eg was from 3.337 to 3.500 eV. The TZO film deposited at a higher temperature exhibited a stronger blue shift phenomenon. The broadening in the bandgap, known as the Burstein–Moss effect, pointed out that the Eg would increase with increasing carrier concentration [22]. This is in accordance with the results of the carrier concentration in Fig. 4.

The hydrogen plasma treatment was performed at 300 °C to further improve the properties of TZO films. Fig. 6 shows the resistivity, Hall mobility, and carrier concentration of TZO films as a function of plasma treatment time. The carrier concentration increased from 2.47×10^{20} to $4.25\times10^{20}\,cm^{-3}$ (or by 72%) as the plasma exposure time varied from 0 (as-deposited) to 90 min. This is attributed to the formation of shallow donors as a result of hydrogen having been inserted into the films [23,24]. The Hall mobility increased from 7.84 to 12.3 cm^2/Vs (or by 57%). The increased mobility may be attributed to the desorption of oxygen species at grain boundaries, which decreases the barrier potential and grain boundary scattering [21]. The film resistivity is the

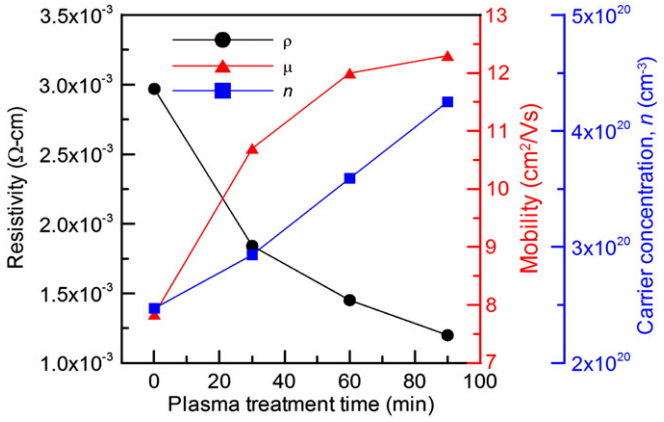

Fig. 6. Resistivity (ρ), Hall mobility (μ) and carrier concentration (n) of the TZO films with various hydrogen plasma treatment times.

combined result of the Hall mobility and the carrier concentration. The film resistivity decreased from 2.91×10^{-3} to 1.20×10^{-3} Ω cm (or a reduction of 60%) after a 90 min plasma treatment. Further extending the plasma treatment time did not result in noticeable changes in film resistivity.

Fig. 7(a) and (b) shows the optical transmittance spectra and optical energy gap (Eg) of TZO films for different plasma treatment times. In Fig. 7(a), the average transmittances in the visible region decreased slightly after plasma treatment and were 83.8%, 78.6%, and 82.6% for the films treated by plasma for 30, 60, and 90 min, respectively. It has been reported that the decrease of optical transmittance of the ZnO:Al film could be ascribed to the enhancement of scattering and absorption of light caused by the increase of surface roughness and carrier concentration [25,26]. In current experiments, the surface roughness and carrier concentration of the films both increase after plasma treatment. Thus, a decrease in the optical transmittance of TZO films is to be expected. The optical bandgaps shown in Fig. 7(b), increased to 3.525 eV as the plasma treatment time was 90 min. After plasma treatment, the blue-shift of the absorption edges is attributed to the Burstein–Moss effect [22]. This is consistent with the increase of carrier concentration in Fig. 6.

Fig. 8 shows the XRD spectra of TZO films for various plasma treatment times. After plasma treatment, the 2θ angle and the FWHM of the (002) diffraction peak remained almost unchanged for the films treated within 60 min as compared to those of the as-deposited one. Therefore, the plasma treatment has a negligible influence on the film structure. This phenomenon is similar with previous research [6,27].

Fig. 9(a)–(d) displays the AFM images of TZO films without and with the plasma treatment for 30–90 min. The measured root mean square (RMS) roughness increased slightly from 0.94 (as-deposited) to 1.23–1.33 nm (plasma-treated). The increase in surface roughness may cause deterioration of the electrical and optical properties [28]. However, the difference in the RMS roughness was relatively small and did not deteriorate the electrical properties of the films in this study. The increase of surface roughness may be attributed to the etching effect of active hydrogen radicals [29]. The increase of surface roughness is helpful for light diffusion and trapping for transparent electrode application in solar cells.

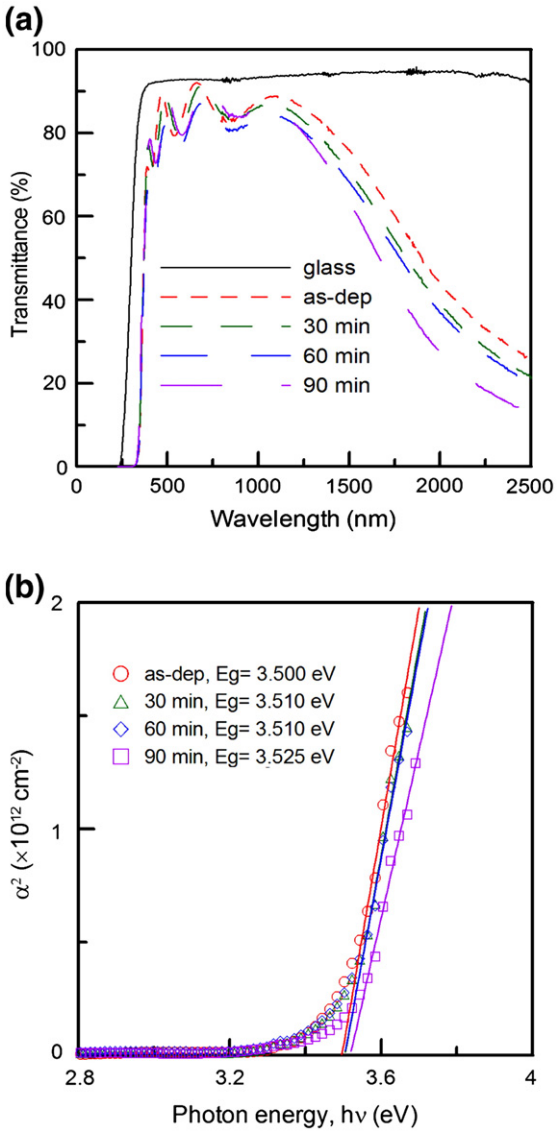

Fig. 7. (a) Optical transmittance spectra and (b) optical energy gap of the TZO films with various hydrogen plasma treatment times.

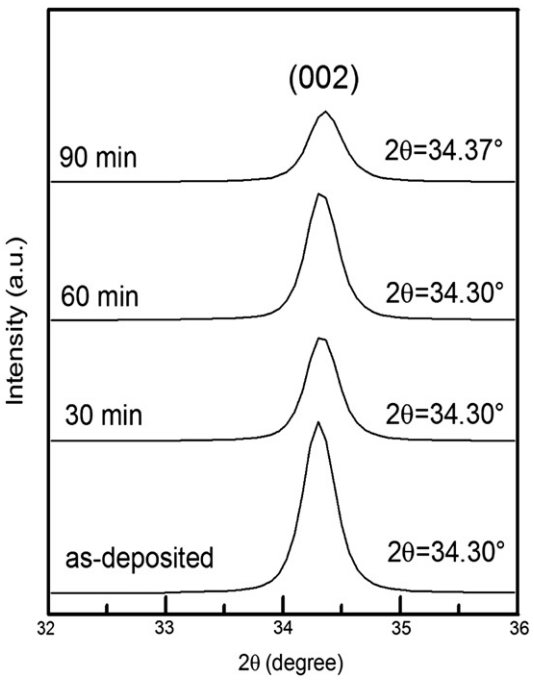

Fig. 8. X-ray diffraction spectra of the TZO films as a function of hydrogen plasma treatment time.

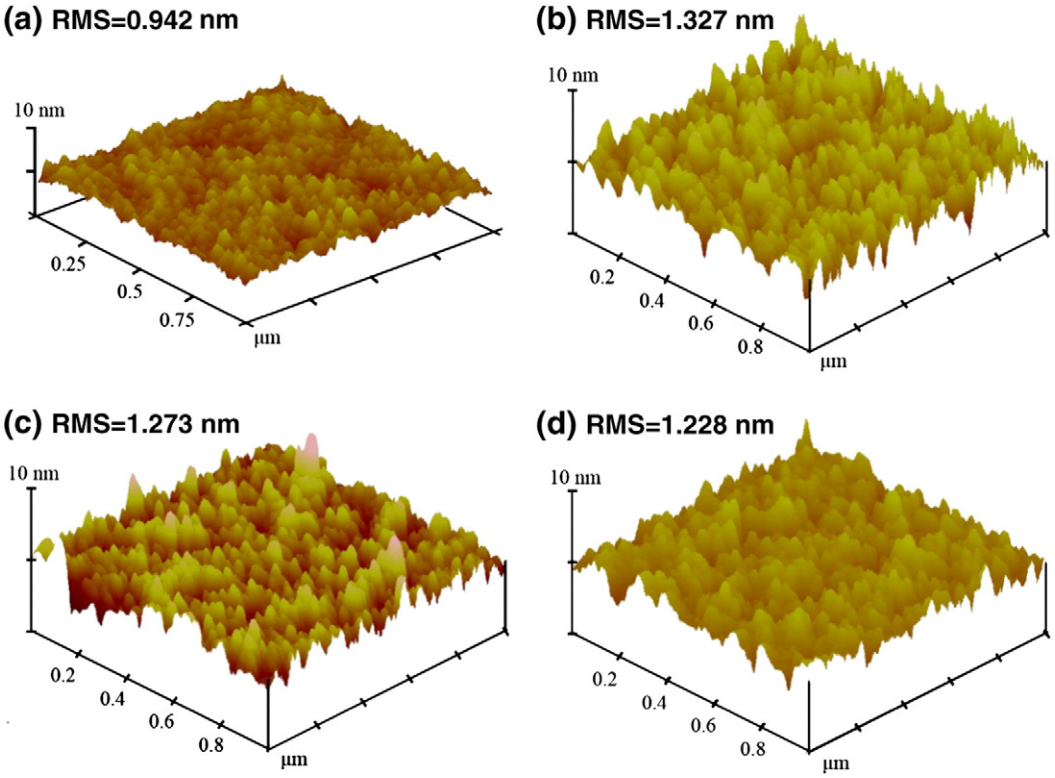

Fig. 9. AFM images of the TZO films over 1 μm × 1 μm area with various hydrogen plasma treatment times: (a) 0 min (as-deposited), (b) 30 min, (c) 60 min, and (d) 90 min.

4. Conclusions

TZO thin films were deposited on glass substrates by RF magnetron sputtering. The structural, electrical, and optical properties of TZO films were strongly dependent on the substrate temperature. From the XRD and SEM analysis, all films exhibited a (002) preferential orientation along the c axis at diffraction angles (2θ) near 34° ± 0.3° and the film crystallinity and crystal size were enhanced with increasing substrate temperature. At a substrate temperature of 300 °C, the resistivity, carrier concentration, and Hall mobility attained the optimal values, 2.95×10^{-3} Ω cm, 2.47×10^{20} cm^{-3}, and 7.84 cm^2/Vs. The optical transmittance increased slightly with the substrate temperature and all the average transmittances in the visible region were more than 82.2%. For the TZO films treated by hydrogen plasma, the crystallinity did not significantly change but the surface roughness slightly increased; the electrical resistivity decreased by 60% to 1.20×10^{-3} Ω cm and the optical bandgap increased by 0.025 eV to 3.525 eV after a 90 min plasma treatment in comparison with the as-deposited films. The improved electrical properties are due to the desorption of negatively charged oxygen species and the formation of shallow donors as a result of hydrogen having been incorporated into the films.

Acknowledgement

This research was partially supported by the National Science Council of ROC (Taiwan) under contract no. NSC 95-2221-E-005-111.

References

[1] W. Dewald, V. Sittinger, W. Werner, C. Jacobs, B. Szyszka, Thin Solid Films 518 (2009) 1085.
[2] I.E. Titkov, L.A. Delimova, A.S. Zubrilov, N.V. Seredova, I.A. Liniichuk, I.V. Grekhov, J. Mod. Opt. 56 (2009) 653.
[3] H.K. Liang, S.F. Yu, H.Y. Yang, Appl. Phys. Lett. 96 (2010) 101116, doi: 10.1063/1.3356221.
[4] J.H. Bae, H.K. Kim, Thin Solid Films 516 (2008) 7866.
[5] T. Minami, H. Nanto, S. Takata, Jpn. J. Appl. Phys. 23 (1984) L280.
[6] H.P. Chang, F.H. Wang, J.Y. Wu, C.Y. Kung, H.W. Liu, Thin Solid Films 518 (2010) 7445.
[7] T. Minami, H. Sato, H. Nanto, S. Takata, Jpn. J. Appl. Phys. 24 (1985) L781.
[8] H.Q. Le, S.K. Lim, G.K.L. Goh, S.J. Chua, J.X. Ong, J. Electrochem. Soc. 157 (2010) H796.
[9] L.P. Peng, L. Fang, X.F. Yang, H.B. Ruan, Y.J. Li, Q.L. Huang, C.Y. Kong, Phys. E 41 (2009) 1819.
[10] H.Q. Le, S.K. Lim, G.K.L. Goh, J. Cryst. Growth 312 (2010) 437.
[11] J.L. Chung, J.C. Chen, C.J. Tseng, Appl. Surf. Sci. 255 (2008) 2494.
[12] J.L. Chung, J.C. Chen, C.J. Tseng, Appl. Surf. Sci. 254 (2008) 2615.
[13] Y.M. Lu, C.M. Chang, S.I. Tsai, T.S. Wey, Thin Solid Films 447–448 (2004) 56.
[14] S.S. Lin, J.L. Huang, D.F. Lii, Mater. Chem. Phys. 90 (2005) 22.
[15] K. Zheng, L. Gu, D. Sun, X.L. Mo, G. Chen, Mater. Sci. Eng., B 166 (2009) 104.
[16] R.G.S. Pala, W. Tang, M.M. Sushchikh, J.N. Park, A.J. Forman, G. Wu, A. Kleiman-Shwarsctein, J. Zhang, E.W. McFarland, H. Metiu, J. Catal. 266 (2009) 50.
[17] C.Y. Tsay, H.C. Cheng, C.Y. Chen, K.J. Yang, C.K. Lin, Thin Solid Films 518 (2009) 1603.
[18] S.S. Lin, J.L. Huang, D.F. Lii, Surf. Coat. Technol. 176 (2004) 173.
[19] K. Koski, J. Holsa, P. Juliet, Thin Solid Films 339 (1999) 240.
[20] G. Sanon, R. Rup, A. Mansingh, Thin Solid Films 190 (1990) 287.
[21] G. Fang, D. Lia, B.L. Yao, Vacuum 68 (2003) 363.
[22] B.E. Sernelius, K.F. Berggren, Z.C. Jim, I. Hamberg, C.G. Granqvist, Phys. Rev. B 37 (1988) 10244.
[23] B.Y. Oh, M.C. Jeong, D.S. Kim, W. Lee, J.M. Myoung, J. Cryst. Growth 281 (2005) 475.
[24] Y.M. Strzhemechny, H.L. Mosbacker, D.C. Look, D.C. Reynolds, C.W. Litton, N.Y. Garces, N.C. Giles, L.E. Halliburton, S. Niki, L.J. Brillson, Appl. Phys. Lett. 84 (2004) 2545.
[25] E.G. Fu, D.M. Zhuang, G. Zhang, Z. Ming, W.F. Yang, J.J. Liu, Microelectron. J. 35 (2004) 383.
[26] J.H. Shin, S.H. Shin, J.I. Park, J. Appl. Phys. 89 (2001) 5199.
[27] N. Ohashi, Y.G. Wang, T. Ishigaki, Y. Wada, H. Taguchi, I. Sakaguchi, T. Ohgaki, Y. Adachi, H. Haneda, J. Cryst. Growth 306 (2007) 316.
[28] D.F. Paraguay, L.W. Estrada, N.D.R. Acosta, E. Andrade, M. Miki-Yoshida, Thin Solid Films 350 (1999) 192.
[29] R. Das, T. Jana, S. Ray, Sol. Energy Mater. Sol. Cells 86 (2005) 207.